

Molecular structure of the substrate-induced thin-film phase of tetracene

Linus Pithan,^{1,2,a)} Dmitrii Nabok,^{1,3} Caterina Cocchi,^{1,3} Paul Beyer,¹ Giuliano Duva,⁴ Joseph Simbrunner,⁵ Jonathan Rawle,⁶ Chris Nicklin,⁶ Peter Schäfer,¹ Claudia Draxl,^{1,3} Frank Schreiber,⁴ and Stefan Kowarik^{1,7,a)}

¹*Institut für Physik, Humboldt-Universität zu Berlin, Newtonstr. 15, 12489 Berlin, Germany*

²*ESRF—The European Synchrotron, 71 Ave. des Martyrs, 38000 Grenoble, France*

³*IRIS Adlershof, HU Berlin, Zum Großen Windkanal 6, 12489 Berlin, Germany*

⁴*Institut für Angewandte Physik, Universität Tübingen, Auf der Morgenstelle 10, 72076 Tübingen, Germany*

⁵*Department of Neuroradiology, Vascular and Interventional Radiology, Medical University Graz,*

Auenbruggerplatz 9, Graz 8036, Austria

⁶*Diamond Light Source Ltd, Harwell Campus, Didcot, Oxfordshire, United Kingdom*

⁷*Bundesanstalt für Materialforschung und–prüfung (BAM), Unter den Eichen 44-46, 12203 Berlin, Germany*

(Received 8 June 2018; accepted 15 September 2018; published online 12 October 2018)

We present a combined experimental and theoretical study to solve the unit-cell and molecular arrangement of the tetracene thin film (TF) phase. TF phases, also known as substrate induced phases (SIPs), are polymorphs that exist at interfaces and decisively impact the functionality of organic thin films, e.g., in a transistor channel, but also change the optical spectra due to the different molecular packing. As SIPs only exist in textured ultrathin films, their structure determination remains challenging compared to bulk materials. Here, we use grazing incidence X-ray diffraction and atomistic simulations to extract the TF unit-cell parameters of tetracene together with the atomic positions within the unit-cell. *Published by AIP Publishing.* <https://doi.org/10.1063/1.5043379>

I. INTRODUCTION

Crystallisation of molecules on a solid surface enables production of thin film devices and coatings. To rationally design specific optical and electronic properties, the thin film knowledge of the crystal structure is crucial. For the deposition of small molecules, it has often been observed that self-organisation on a surface results in a new polymorphic form different from the molecular bulk crystal structure.¹ These so called thin film (TF) phases or substrate induced phases (SIP) are defined as a structure extending both within the film plane as well as out-of-plane. According to this definition, a monolayer structure or surface reconstruction does not constitute a substrate-induced polymorph. Rather, the structure must extend over multiple molecular dimensions in all directions (in- and out-of-plane) in order to be a new polymorph. Although TF phases different from bulk phases have been detected for many molecules, only for a limited number of TF phases the complete structure including molecular arrangement is known. Therefore, the investigation of a prototypical and well-studied system such as tetracene contributes to a better understanding of the general properties of TF phases, e.g., regarding the role of molecular shape, growth mechanisms, and thermodynamics of TF phases.

TF phases have been found for a number of molecules such as diindenoperylene,² alpha-sexithiophene,³ sexiphenyl,⁴ or pentacene^{5–8} and we refer to a recent review of substrate

induced polymorphs by Jones *et al.* (Ref. 1) for a more complete overview. Molecular TF phases are mostly solved by grazing incidence X-ray diffraction (GIXD), which is challenging because the amount of scattering material is small and indexation procedures are not automated as in the case of (bulk) single crystal Bragg reflections.⁹ The most studied example of a substrate induced polymorph is the TF phase of pentacene, which, as a larger member of the acenes, is closely related to tetracene and a benchmark material for organic semiconductor devices.

Pentacene exhibits the coexistence of TF and high temperature (HT) bulk phases in ultrathin layers.¹⁰ In both phases, there are two molecules in a herringbone arrangement within the triclinic unit-cell.^{5,11} The pentacene TF phase on SiO_x consists of nearly upright standing molecules, which are slightly tilted with respect to the substrate surface normal. Compared to the low temperature bulk phase,¹² this tilt is reduced in the TF phase, leading to changes in electronic and excitonic coupling between molecules and therefore different band structures and optical spectra.^{7,11} Especially for electronic applications, e.g., in organic field effect transistors (OFETs), the TF phase is important because the conducting channel is located at the interface between SiO_x and the organic semiconductor.¹³ Indeed the pentacene SIP has been found to increase the charge carrier mobility above the bulk polymorph values.¹⁴ Also, the specific structure and packing is crucial for the optical properties of organic crystals.^{15–19} Due to the similar packing motif, bulk and TF phase can coexist in the film, and transitions from TF to bulk phase can be induced via temperature and aging.^{10,20,21}

^{a)}Authors to whom correspondence should be addressed: linus.pithan@esrf.fr and stefan.kowarik@bam.de

Tetracene ($C_{18}H_{12}$) molecules, which consist of four fused benzene rings as opposed to five in pentacene (see Fig. 1) are also known to grow in a TF phase. Different bulk phases,^{22–24} interesting growth behavior,²⁵ and a surface reconstruction of tetracene single crystals have been observed.²⁶ Previously, the coexistence of two phases within tetracene thin films was identified by the characteristic (001) d -spacing.^{27–29} Recently, Nahm and co-worker followed this phase coexistence of a TF and bulk phase with time-resolved *in situ* X-ray scattering, showing that there are three stages of initially pure TF, mixed phase, and eventually pure bulk phase growth.³⁰ Also the unit-cell of the tetracene TF phase was determined for the first time by Nahm and Engstrom.³⁰ However, the molecular arrangement *within* the unit-cell remained unknown. The molecular arrangement in the TF phase of tetracene is needed for a detailed characterisation and analysis, also from a theoretical perspective, of the charge carrier transport and the band structure as well as optical properties and excitonic coupling between molecules.^{15,31} Indeed, structural changes due to the surface relaxation in tetracene single crystals have been shown to result in significantly different band structures.²⁶ Also, the singlet fission rates in tetracene have been found to differ between the thin film and bulk polymorphs³² so that the exact TF structure can contribute to a better understanding of singlet-fission mechanisms in tetracene solar cells.³³

In this work, we report the crystallographic unit-cell and molecular arrangement of the tetracene TF phase on SiO_x .

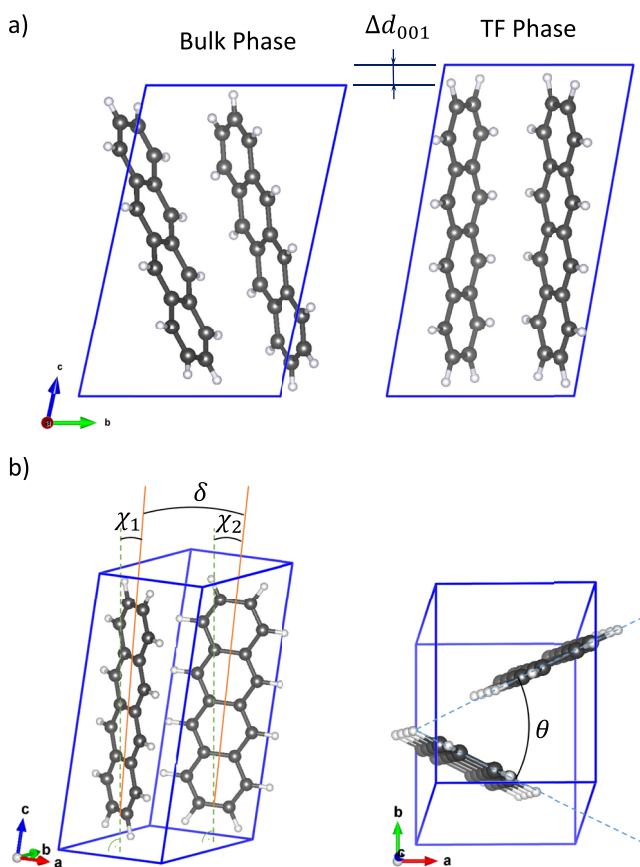


FIG. 1. (a) Orientation of tetracene molecules in bulk and thin film phase. (b) The tilt angles χ_1 and χ_2 define the angle of the long molecular axes (orange) to the c^* direction (\perp ab -plane, dashed). δ is the angle between the long axes of the two molecules within the unit-cell and θ the herring bone angle.

We derive the results from X-ray reflectivity (XRR) and grazing incidence x-ray diffraction (GIXD) measurements combined with atomistic simulations based on force-field and density-functional-theory (DFT) calculations. This combined approach unravels the atomic coordinates and molecular arrangement within the unit-cell, going beyond the determination of simple out-of-plane lattice spacing or pure cell geometry, and hence, is more generally applicable for crystalline organic thin films.

II. METHODS

A. Experimental

We use a portable organic molecular beam deposition (OMBD) setup operated at a base pressure of 10^{-7} mbar to grow tetracene thin films at a nominal growth rate of ≈ 1 Å/min via thermal evaporation from a crucible. During the growth, the substrate temperature is kept at 250 K to ensure a sufficiently high sticking coefficient and prevent significant re-evaporation. The growth rate is monitored by a quartz crystal microbalance (QCM). The films are grown to a nominal thickness of 20 nm. GIXD and XRR measurements were performed *in situ* at room temperature at the I07 beamline located at the Diamond Light Source using an energy of 13 keV and a Pilatus 100k area detector.³⁴ The presented q -space map has been stitched from more than 100 individual detector images acquired at a sample detector distance of 0.92 m. For scanning electron microscopy, a Zeiss Gemini 500 has been used.

B. Computational determination of molecular coordinates

To find the equilibrium orientation of molecules in the unit-cell adopted from the experiment, we employ a variant of the Modified Genetic Algorithm for Crystals and Clusters (MGAC).³⁵ This global optimization technique has been successfully applied for solving the packing of rod-like organic molecules in a number of materials.^{36,37} Computationally, the optimization procedure consists of two steps. During the first step, the two non-equivalent tetracene molecules included in the unit-cell (see Fig. 1) are considered as rigid bodies, described by 6 Euler angles. We assume the herringbone-type of molecular packing in the ab -plane which determines the position of the molecular centre-of-masses. The goal of this step is to explore efficiently the complex potential surface and suggest the “first-guess” crystal structures. Taking into account predominantly van der Waals intermolecular interactions, the global optimization search is performed minimizing the total energy obtained by employing the Merck Molecular Force Field (MMFF)³⁸ as implemented in the TINKER molecular modeling software.³⁹ In the second step, the local minima with lowest energy from the previous step are further refined in the framework of density-functional-theory (DFT) with the optB86b-vdW⁴⁰ exchange-correlation functional, as implemented in VASP (Vienna ab initio simulation package).^{41–44} A plane-wave energy cutoff of 500 eV and a $4 \times 3 \times 2$ k-point grid are used to ensure high quality of the ground-state calculations. This second step is necessary to provide an exhaustive structure prediction, taking

into account both intra- and inter-molecular interactions in a quantum-mechanical framework.

III. RESULTS

Our analysis is structured as follows: First, we characterise the out-of-plane lattice spacing by XRR. In a second step, we find unit-cell parameters that fit the observed GIXD reflections. Then we determine the molecular arrangement within the experimentally determined unit-cell. Finally, we verify the computed atomic positions through a comparison of measured diffraction intensities and those from calculating the structure factor.

In Fig. 2, the *in situ* XRR measurement on a 20 nm tetracene film on a silicon wafer with native oxide is shown. The (00L) Bragg reflections up to 4th order indicate high structural order and the doublet structure of each reflection is a clear indication of coexisting thin film and bulk phase. As commonly observed in organic thin films and polyacene films, in particular, the (001) plane of the molecular unit-cell forms the contact plane with the underlying substrate. From the (00L) reflections, we determine the lattice spacing of each phase along c^* , which is the projection of the unit-cell vector c onto the ab -plane normal. The (001) lattice spacing for the bulk phase is $d_{(001)B} = (12.16 \pm 0.03) \text{ \AA}$, which is compatible with the crystal structure published by Holmes²² and for the TF phase under investigation we find $d_{(001)TF} = (12.93 \pm 0.03) \text{ \AA}$. No thickness oscillations due to interference (Kiessig fringes) are observed in XRR, both during thin film growth as well as in post-growth measurement, indicating a high surface roughness of the film. This finding is confirmed by *ex situ* SEM images (inset Fig. 2), where we additionally find that the film partially de-wets. This behavior has also been observed by Nahm and Engstrom at higher deposition rates for films grown by supersonic beam deposition.⁴⁵

To determine also the in-plane unit-cell vectors, we analyze the GIXD diffraction pattern of the textured film [Fig. 3(a)]. We separate the reflections resulting from the bulk polymorph and those that stem from the thin film structure.

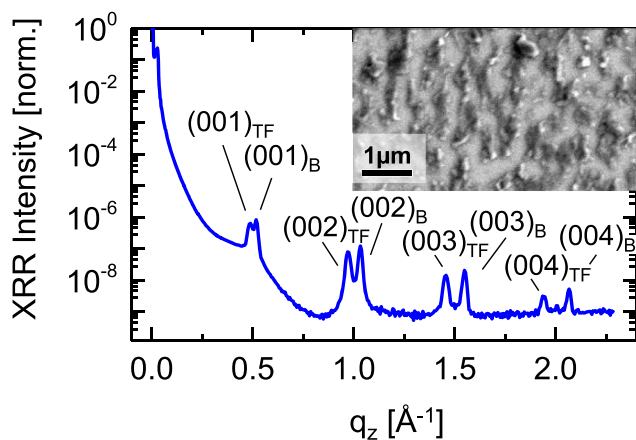


FIG. 2. X-ray reflectivity (XRR) curve of a 20 nm thick tetracene film, showing pairs of (00L) reflections. The double peaks indicate the coexistence of a thin film (TF) and bulk phase (B) in the film. Inset: SEM image of the thin film.

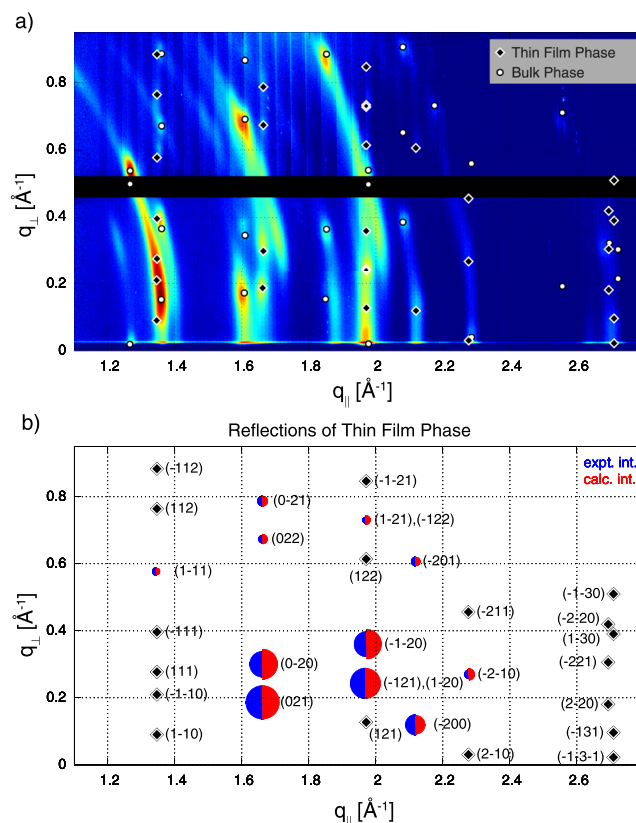


FIG. 3. (a) q -space map recorded in GIXD geometry (intensity increasing from blue to red). Positions of reflections according to the TF and bulk phases are indicated. (b) Indexing of TF reflections based on our unit-cell. The experimental reflection intensity (indicated by circle diameter) agrees with the calculated intensity based on the molecular coordinates.

For the determination of the unit-cell based on GIXD diffraction data, a set of hypothetical diffraction patterns has been generated by varying the unit-cell parameters starting from the known tetracene bulk crystal structure to find the best fit corresponding to the experimental findings.⁴⁶ Since the reciprocal unit-cell vector c^* has been previously determined by XRR, it is used as constraint in the above described fitting procedure. Following this approach, we derive unit-cell parameters of $a = 5.93 \pm 0.05 \text{ \AA}$, $b = 7.56 \pm 0.05 \text{ \AA}$, $c = 13.17 \pm 0.03 \text{ \AA}$, $\alpha = 79.8^\circ \pm 0.5^\circ$, $\beta = 86.8^\circ \pm 0.5^\circ$, and $\gamma = 90.1^\circ \pm 0.3^\circ$ with a unit-cell volume of 580.1 \AA^3 . Based on these unit-cell parameters, we simulate the atomic positions with the two-step calculation procedure described above. The resulting molecular arrangement is characterised by a set of angles [Fig. 1(b)], which are denoted according to the nomenclature from the literature.^{7,11} χ_1 and χ_2 describe the tilt of the long molecular axis of each molecule with respect to c^* (the ab -plane normal). The angle θ represents the herringbone angle, and δ describes the difference in the orientation of the two long molecular axes. The calculated orientation of the two molecules in the unit-cell corresponds to $\theta = 53.7^\circ$, $\chi_1 = 5.9^\circ$, $\chi_2 = 4.8^\circ$, and $\delta = 1.2^\circ$ (Table I). The computed atomic positions are provided in the [supplementary material](#) as a cif-file.

A. Structure-factor analysis for validation

To validate the atomic positions resulting from the calculations, we compute the theoretical diffraction intensities of

TABLE I. Unit-cell parameters and angles defining the molecular orientation within the unit-cell for tetracene and pentacene polymorphs.

	Tetracene TF (this work)	Tetracene TF ³⁰	Tetracene bulk ²²	Pentacene TF ^{7,11}	Pentacene bulk ^{11,12}
Unit-cell					
a (Å)	5.93 ± 0.05	5.92	6.06	5.92	6.06
b (Å)	7.56 ± 0.05	7.6	7.84	7.54	7.90
c (Å)	13.17 ± 0.03	13.2	13.01	15.63	15.01
α (deg)	79.8 ± 0.5	79.8	77.1	81.5	81.6
β (deg)	86.8 ± 0.5	86.4	72.1	87.2	77.2
γ (deg)	90.1 ± 0.3	89.6	85.8	89.9	85.5
V (Å ³)	580.1	583.3	572.9	689.2	692.6
Molecular orientation within the unit-cell					
θ (deg)	53.7	N.A.	51.4	54.1	52.6
χ ₁ (deg)	5.9	N.A.	23.7	3.1	22.1
χ ₂ (deg)	4.8	N.A.	21.3	2.9	20.3
δ (deg)	1.2	N.A.	2.8	0.3	2.9

the TF phase for a comparison with experimental diffraction intensities [Fig. 3(b)]. The theoretical diffraction intensity for a certain Bragg reflection $I_{\text{hkl}} \propto |F_{\text{hkl}}|^2$ is given by the structure factor

$$F_{\text{hkl}} = \sum_a f_a e^{i\mathbf{q}_{\text{hkl}} \cdot \mathbf{r}_a}.$$

Here, f_a represents the atomic form factor and \mathbf{r}_a the position of each individual atom a within the unit-cell as determined theoretically.⁴⁷ To account for the given experimental conditions, correction factors have to be applied before comparison of calculated and experimental intensities. We apply polarization and Lorentz correction and also consider the interception angle of the scattering rods as discussed in detail in Ref. 48.

In order to extract the experimental intensities from the recorded GIXD reflection patterns, 2d Gaussian profiles are fitted to the reflections directly in the 2d detector images before distortion correction.⁶ Where necessary, a background correction is applied in order to fully separate the TF reflections from neighbouring reflections of the bulk phase. Using the strong (021) reflection for normalisation, the remaining ten reflections in Fig. 3(b) show a satisfactory agreement between computed and experimentally observed intensities (the average deviation between simulated and experimental intensities is $13\% \pm 9\%$).

Table I summarises the results of this study and additionally draws the comparison to known crystal structures of tetracene and the respective structures of pentacene. The comparison between tetracene and pentacene unit-cells reveals great similarities, the main difference being the height of the unit-cell in the c direction due to the additional benzene-ring in the pentacene molecule. Regarding the volumes of the unit-cells, the TF phase of pentacene features a slightly reduced value compared to the bulk phase. By contrast, we find that for tetracene it is slightly increased in the TF phase compared to what is known from the bulk phase. Our observation of an increased unit-cell volume of the tetracene SIP is in line with the observed behavior of most molecular materials with a SIP.¹

Great similarity is also found for the molecular arrangement in tetracene and pentacene polymorphs. Thus, in the bulk phase both tetracene and pentacene molecules are tilted in the ab -plane by around 20° , and the corresponding tilt in the TF polymorphs is significantly smaller, corresponding to more upright standing molecules. Interestingly, for tetracene, this angle χ is ca. 3° larger than in pentacene. This is likely due to the greater length of pentacene molecules that results in more attractive interactions between neighboring pentacene molecules. To validate our numerical procedure for the equilibrium molecular arrangement, we have also applied the optimization algorithm to the known bulk phase of tetracene. The resulting molecular geometry parameters are $\theta = 51.0^\circ$, $\chi_1 = 23.4^\circ$, $\chi_2 = 21.0^\circ$, and $\delta = 3.1^\circ$. Comparing these values with those in Table I, one finds very good agreement between the simulated and experimentally measured geometries, demonstrating the predictive power of our approach.

IV. CONCLUSIONS

In this work, we have solved the structure of and the atomic positions within the tetracene thin film phase. The obtained unit-cell agrees with a recent report.³⁰ Here, however, we go beyond the cell geometry and also determine the molecular arrangement and the atomic coordinates within the unit-cell. The combined experimental and computational approach presented here can be readily extended to other molecular species with surface-induced crystal phases. This is particularly important in the context of molecular (opto-) electronics where knowledge of the molecular arrangement in thin films crucially impacts opto-electronic properties, including the exciton binding strength. With the model system tetracene, our results lead to a better understanding of the structure-function relationship of molecular TF phases in view of their charge carrier mobilities, optical spectra, and singlet fission characteristics. This understanding will contribute to an optimized design of devices such as organic transistors and singlet-fission solar cells.

SUPPLEMENTARY MATERIAL

See [supplementary material](#) for crystallographic data (cif file) that contains the thin film crystal structure of tetracene.

ACKNOWLEDGMENTS

We thank the Diamond Light Source for access to beamline I07. Furthermore we thank Roland Resel and Andreas Opitz for their support and Alexander Gerlach as well as Anton Zykov for fruitful discussions. We acknowledge support from the DFG collaborative research center SFB 951 and G.D. acknowledges the support from the Carl-Zeiss-Stiftung. F.S. acknowledges support from the DFG.

- ¹A. O. F. Jones, B. Chattopadhyay, Y. H. Geerts, and R. Resel, *Adv. Funct. Mater.* **26**, 2233 (2016).
- ²S. Kowarik, A. Gerlach, S. Sellner, L. Cavalcanti, O. Konovalov, and F. Schreiber, *Appl. Phys. A* **95**, 233 (2008).
- ³A. Moser, I. Salzmann, M. Oehzelt, A. Neuhold, H. G. Flesch, J. Ivanco, S. Pop, T. Toader, D. R. T. Zahn, D. M. Smilgies, and R. Resel, *Chem. Phys. Lett.* **574**, 51 (2013).
- ⁴R. Resel, N. Koch, F. Meghdadi, G. Leising, L. Athouel, G. Froyer, and F. Hofer, *Cryst. Res. Technol.* **36**, 47 (2001).
- ⁵S. Schiefer, M. Huth, A. Dobrinevski, and B. Nickel, *J. Am. Chem. Soc.* **129**, 10316 (2007).
- ⁶S. C. B. Mannsfeld, A. Virkar, C. Reese, M. F. Toney, and Z. Bao, *Adv. Mater.* **21**, 2294 (2009).
- ⁷D. Nabok, P. Puschnig, C. Ambrosch-Draxl, O. Werzer, R. Resel, and D. M. Smilgies, *Phys. Rev. B* **76**, 235322 (2007).
- ⁸H. Yoshida, K. Inaba, and N. Sato, *Appl. Phys. Lett.* **90**(18), 181930 (2007).
- ⁹S. Kowarik, *J. Phys.: Condens. Matter* **29**, 043003 (2017).
- ¹⁰C. Westermeier, A. Cernescu, S. Amarie, C. Liewald, F. Keilmann, and B. Nickel, *Nat. Commun.* **5**, 4101 (2014).
- ¹¹C. Ambrosch-Draxl, D. Nabok, P. Puschnig, and C. Meisenbichler, *New J. Phys.* **11**, 125010 (2009).
- ¹²R. B. Campbell, J. M. Robertson, and J. Trotter, *Acta Crystallogr.* **15**, 289 (1962).
- ¹³R. Lassnig, B. Striedinger, M. Hollerer, A. Fian, B. Stadlober, and A. Winkler, *J. Appl. Phys.* **116**, 114508 (2014).
- ¹⁴C. D. Dimitrakopoulos, A. R. Brown, and A. Pomp, *J. Appl. Phys.* **80**, 2501 (1996).
- ¹⁵S.-H. Lim, T. G. Bjorklund, F. C. Spano, and C. J. Bardeen, *Phys. Rev. Lett.* **92**, 107402 (2004).
- ¹⁶U. Heinemeyer, K. Broch, A. Hinderhofer, M. Kytka, R. Scholz, A. Gerlach, and F. Schreiber, *Phys. Rev. Lett.* **104**, 257401 (2010).
- ¹⁷I. Meyenburg, T. Breuer, A. Karthäuser, S. Chatterjee, G. Witte, and W. Heimbrod, *Phys. Chem. Chem. Phys.* **18**, 3825 (2016).
- ¹⁸P. Puschnig, K. Hummer, C. Ambrosch-Draxl, G. Heimel, M. Oehzelt, and R. Resel, *Phys. Rev. B* **67**, 235321 (2003).
- ¹⁹K. Hummer, P. Puschnig, and C. Ambrosch-Draxl, *Phys. Rev. Lett.* **92**, 147402 (2004).
- ²⁰A. Moser, J. Novák, H.-G. Flesch, T. Djuric, O. Werzer, A. Haase, and R. Resel, *Appl. Phys. Lett.* **99**, 221911 (2011).
- ²¹T. Ji, S. Jung, and V. K. Varadan, *Org. Electron.* **9**, 895 (2008).
- ²²D. Holmes, S. Kumaraswamy, A. J. Matzger, and K. P. C. Vollhardt, *Chem. - Eur. J.* **5**, 3399 (1999).
- ²³E. Venuti, R. G. Della Valle, L. Farina, A. Brillante, M. Masino, and A. Girlando, *Phys. Rev. B* **70**, 104106 (2004).
- ²⁴U. Sondermann, A. Kutoglu, and H. Bassler, *J. Phys. Chem.* **89**, 1735 (1985).
- ²⁵M. Voigt, S. Dorsfeld, A. Volz, and M. Sokolowski, *Phys. Rev. Lett.* **91**, 026103 (2003).
- ²⁶H. Morisaki, T. Koretsune, C. Hotta, J. Takeya, T. Kimura, and Y. Wakabayashi, *Nat. Commun.* **5**, 5400 (2014).
- ²⁷B. Gompf, D. Faltermeier, C. Redling, M. Dressel, and J. Pflaum, *Eur. Phys. J. E* **27**, 421 (2008).
- ²⁸S. Milita, C. Santato, and F. Ciccoira, *Appl. Surf. Sci.* **252**, 8022 (2006).
- ²⁹S. Milita, M. Servidori, F. Ciccoira, C. Santato, and A. Pifferi, *Nucl. Instrum. Methods Phys. Res., Sect. B* **246**, 101 (2006).
- ³⁰R. K. Nahm and J. R. Engstrom, *J. Chem. Phys.* **146**, 052815 (2017).
- ³¹K. Hummer and C. Ambrosch-Draxl, *Phys. Rev. B* **72**, 205205 (2005).
- ³²D. H. Arias, J. L. Ryerson, J. D. Cook, N. H. Damrauer, and J. C. Johnson, *Chem. Sci.* **7**, 1185 (2016).
- ³³T. C. Wu, N. J. Thompson, D. N. Congreve, E. Hontz, S. R. Yost, T. Van Voorhis, and M. A. Baldo, *Appl. Phys. Lett.* **104**, 193901 (2014).
- ³⁴C. Nicklin, T. Arnold, J. Rawle, and A. Warne, *J. Synchrotron Radiat.* **23**, 1245 (2016).
- ³⁵V. E. Bazterra, M. B. Ferraro, and J. C. Facelli, *J. Chem. Phys.* **116**, 5984 (2002).
- ³⁶I. Salzmann, D. Nabok, M. Oehzelt, S. Duhm, A. Moser, G. Heimel, P. Puschnig, C. Ambrosch-Draxl, J. P. Rabe, and N. Koch, *Cryst. Growth Des.* **11**, 600 (2011).
- ³⁷I. Salzmann, A. Moser, M. Oehzelt, T. Breuer, X. Feng, Z. Juang, D. Nabok, R. G. Della Valle, S. Duhm, G. Heimel, A. Brillante, E. Venuti, I. Bilotti, C. Christodoulou, J. Frisch, P. Puschnig, C. Draxl, and G. Witte, *ACS Nano* **6**, 10874 (2012).
- ³⁸T. A. Halgren, *J. Comput. Chem.* **17**, 520 (1996).
- ³⁹J. W. Ponder, *TINKER: Software Tools for Molecular Design*, 5th ed. (Washington University School of Medicine, Saint Louis, MO, 2010).
- ⁴⁰J. Klime, D. R. Bowler, and A. Michaelides, *Phys. Rev. B* **83**, 195131 (2011).
- ⁴¹G. Kresse and J. Hafner, *Phys. Rev. B* **47**, 558 (1993).
- ⁴²G. Kresse and J. Hafner, *J. Phys.: Condens. Matter* **6**, 8245 (1994).
- ⁴³G. Kresse and J. Furthmüller, *Phys. Rev. B* **54**, 11169 (1996).
- ⁴⁴G. Kresse and J. Furthmüller, *Comput. Mater. Sci.* **6**, 15 (1996).
- ⁴⁵R. K. Nahm and J. R. Engstrom, *J. Phys. Chem. C* **120**, 7183 (2016).
- ⁴⁶L. Pithan (2018). "GIXDtools," Zenodo. <https://doi.org/10.5281/zenodo.1414322>
- ⁴⁷J. Als-Nielsen and D. McMorrow, *Elements of Modern X-Ray Physics* (John Wiley & Sons, Inc., Hoboken, NJ, USA, 2011).
- ⁴⁸D. M. Smilgies, *Rev. Sci. Instrum.* **73**, 1706 (2002).